JOURNAL OF SOLID STATE CHEMISTRY **141,** 56–63 (1998)
ARTICLE NO. SC987914

Cation Migration and Coercivity in Mixed Copper–Cobalt Spinel Ferrite Powders

Ph. Tailhades, C. Villette, and A. Rousset

Laboratoire de Chimie des Matériaux Inorganiques, Université Paul Sabatier, 118 route de Narbonne, 31062 Toulouse Cedex 4, France

G. U. Kulkarni, K. R. Kannan, and C. N. R. Rao

Chemistry and Physics of Materials Unit, Jawaharlal Nehru Centre for Advanced Scientific Research, Jakkur P.O., Bangalore 560 064, India

and

M. Lenglet

Laboratoire d'Analyse Spectroscopique et de Traitement de Surface des Matériaux, Université de Rouen, IUT, 76821 Mont-Saint-Aignan Cedex, France

Received December 8, 1997; in revised form May 27, 1998; accepted June 3, 1998

Mixed cobalt–copper spinel ferrites $Co_xCu_{1-x}Fe_2O_4$ with acicular shape, prepared from oxalate precursors at moderate temperatures, have been investigated by several techniques to relate the coercivity with structure. The cation distribution in these ferrites is sensitive to the thermal history of the samples. Cation migration occurs during annealing in the 200–600°C range in samples quenched from 710°C and in the 350–600°C range in slowly cooled samples. Because of shape anisotropy, tetragonal distortion, and directional order, coercivities from about 1500 to 4000 Oe are obtained in these ferrites. © 1998 Academic Press

INTRODUCTION

Copper ferrites of formula $CuFe_2O_{4-\delta}$ are distinguished from other spinel ferrites because of the tetragonally distorted spinel structure exhibited by them, on the one hand, and the inability to have a cation/oxygen ratio higher than 3/4, on the other. Close to thermodynamic equilibrium at room temperature, the copper ferrites may be described by the structural formula $Fe^{3+}[Fe^{3+}Cu^{2+}]O_4^{2-}$, in which the octahedral cations are placed inside square brackets (1–3). The spinel lattice is thus highly distorted ($c/a \sim 1.06$) because of a cooperative Jahn–Teller effect arising from the octahedral cupric ions (4, 5). Part of the Cu^{2+} ions can be frozen in tetrahedral sites when the ferrites are quenched in air from temperatures higher than 400°C (1, 3, 6, 7). The resulting ferrites show a smaller tetragonal distortion since a great proportion of the cupric ions are located on tetrahedral sites. Moreover, quenching treatments in air from temperatures higher than 750°C lead to the formation of oxygen-deficient spinel ferrites, the nonstoichiometry arising from the reduction of some of the Cu^{2+} ions to Cu^{+} ions (8, 9). Some authors (7, 9) consider that the Cu^{+} ions are located in the interstitial sites (i.e., sites normally not occupied in the spinel structure).

Annealing treatments can modify the cationic distribution and the oxidation states of the ions in copper ferrites. In particular, Cu^{2+} ion migration from the tetrahedral to the octahedral sites and Cu^{+} oxidation can occur around 250–350 and 350–420°C, respectively, when the samples are heated at 10°C/min (9). When placed in octahedral sites, the Cu^{2+} ions need greater energy to migrate to the tetrahedral sites and such a migration occurs above 400–450°C for comparable heating rates (7).

It has been shown that the coercivity of fine powders of copper ferrites or mixed cobalt–copper ferrites is strongly dependent on the distortion of the spinel lattice, the coercive force increasing with the distortion (7). It is also known that directional ordering (10, 11) can occur in cobalt-containing spinel ferrites due to the mobility of the cations at moderate temperatures (12–15). This is essentially a short-range ordering of the cations on the octahedral sites along the local magnetization direction which allows minimization of the energy of the magnetic material. The anisotropy induced due to directional order is a property related to the metastable reorganization of local atomic surroundings, which can lead to an increase in the coercivity for acicular single-domain particles containing cations with strong magnetocrystalline anisotropy such as Co^{2+} and Fe^{2+}. A method for examining the directional order consists of plotting the

0022-4596/98 $25.00

coercivity, measured at room temperature, after each step of annealing from 25°C to the Curie temperature of the sample (16). The temperature at which directional order occurs in fine powders of spinel ferrites is generally in the 200–300°C range. In samples free of directional order, it is revealed by the increase in the coercivity. Above 300°C, the metastable order is progressively destroyed and a decrease in coercivity is observed in the $H_c = f(T_{\text{annealing}})$ curves.

We have attempted to correlate the variation in the magnetic properties with the structural changes in finely divided cobalt–copper ferrites. For this purpose, we have investigated the cationic migration in the spinel lattice due to annealing in quenched and slowly cooled (10°C/h) acicular fine powders of $Co_xCu_{1-x}Fe_2O_4$ ($0 \leq x \leq 1$) ferrites.

EXPERIMENTAL

$CuFe_2O_4$ and $Co_xCu_{1-x}Fe_2O_4$ particles were prepared by a *chimie douce* method using oxalate precursors. The method consists of two main stages. In the first, a concentrated solution of cupric, cobaltous, and ferrous chlorides is reacted with an oxalic acid solution to get a precipitate of oxalates. The metallic salts were initially dissolved in a mixture of water, ethylene glycol, and hydrochloric acid, while the oxalic acid was dissolved in an ethyl alcohol (95%) and water (5%) mixture. These alcoholic solutions, which have dielectric constants lower than that of pure water, help to obtain smaller oxalate particles than in aqueous medium alone (17). Moreover, in pure water, the chemical precipitation of copper and iron ions by oxalic acid leads to the formation of α-$FeC_2O_4 \cdot 2H_2O$ (18) or α-$(Fe_{1-y}Co_y)C_2O_4 \cdot 2H_2O$ and $CuC_2O_4 \cdot H_2O$ (19). On the other hand, in the aqueous alcohol medium, a pure mixed oxalate is obtained, in spite of the structural differences between iron and copper oxalates (20).

The X-ray diffraction patterns of the oxalates prepared in this manner revealed only one system of lines, similar to the diagram of β-$FeC_2O_4 \cdot 2H_2O$ described by Deyrieux *et al.* (18). Evidence for the substitution of iron by copper is provided by the modification of the lattice constants. The unit cell parameters are $a = 1.206$ nm, $b = 0.547$ nm, and $c = 1.566$ nm with a standard deviation of ~ 0.006 nm for a mixed oxalate with Cu:Fe = 1:2, instead of $a = 1.226$ nm, $b = 0.557$ nm, and $c = 1.548$ for β-$FeC_2O_4 \cdot 2H_2O$. Substitution of copper by cobalt is revealed by the modification of the lattice constants, higher cobalt contents leading to an increase in the a and b parameters and a decrease in the c parameters. High cobalt content also leads to a decrease in the length and the diameter of the particles. The weight losses measured by thermogravimetry after the decomposition of the mixed oxalates into $Cu_{1-x}Co_xFe_2O_4$ show that these salts can be described by the general formula $Cu_{(1-x)/3}Co_{x/3}Fe_{2/3}C_2O_4 \cdot 2H_2O$.

TABLE 1
Chemical Compositions and *c*/*a* Ratios of the $Cu_{1-x}Co_xFe_{2-x}O_4$ Samples

	$1-x$									
	1		0.85		0.4		0.2		0	
	SC	Q	SC	Q	SC	Q	SC	Q	SC	Q
c/a	1.06	1.049	1.047	1	1	1	1	1	1	1

In the second stage, the oxalate precursors were slowly decomposed in air at 710°C for 4 h and quenched (Q samples) or slowly cooled at -10°C/h (SC samples). The resulting products were monophasic with tetragonal or cubic spinel structures (Table 1). The heat treatment used allows the pseudomorphic transformation of the acicular oxalate crystals, leading to acicular ferrite particles (Fig. 1) with sizes directly linked to the sizes of the corresponding precursors particles. The length and the diameter of the spinel oxide particles were lower when the Cu content decreased (Fig. 1). However, for all the samples prepared, the heat treatment was adjusted to obtain a mean crystallite size, close to 45 nm, as measured from X-ray line broadening using the Scherrer method.

The morphology of the powders was determined by scanning electron microscopy (SEM) using a JEOL JSM 6400. To verify their purities, all samples were analyzed by X-ray diffraction using a Siemens X-ray diffraction unit (Model D501) and a cobalt target. Differential scanning calorimetry (DSC) experiments were carried out in air with a SETARAM DSC 111G. These measurements were made on about 65 mg of powder. Magnetic properties were measured on a S2IS M2000 pulsed-field magnetometer, which allows the application of a maximum magnetic field of 25 kOe. The measurements were done at room temperature on packed samples (packing density close to 1 g/cm^3).

Diffuse reflectance spectra in the UV–visible and near-infrared regions were obtained with a Perkin-Elmer Lamda 9 spectrophotometer equipped with an integrating sphere accessory (the integrating sphere was coated with $BaSO_4$ and the spectra were referenced against $BaSO_4$). For a more precise comparison in the near-infrared region, the spectra of cobalt ferrites were converted to the Kubelka–Munk remission function by $F(R) = (1-R)^2/2R = k/s$, where R is the reflectance and k is the absorption coefficient. Assuming that the scattering coefficient s has a small variation with the wavelength over the range of interest, the shapes of the remission function and absorption spectrum are identical.

^{57}Fe Mössbauer spectra of the samples were recorded employing a constant-acceleration spectrometer using a 25-Ci ^{57}Co source in a Pd matrix (Amersham Corp., U.K.). Absolute velocity calibration was done with an Fe foil of

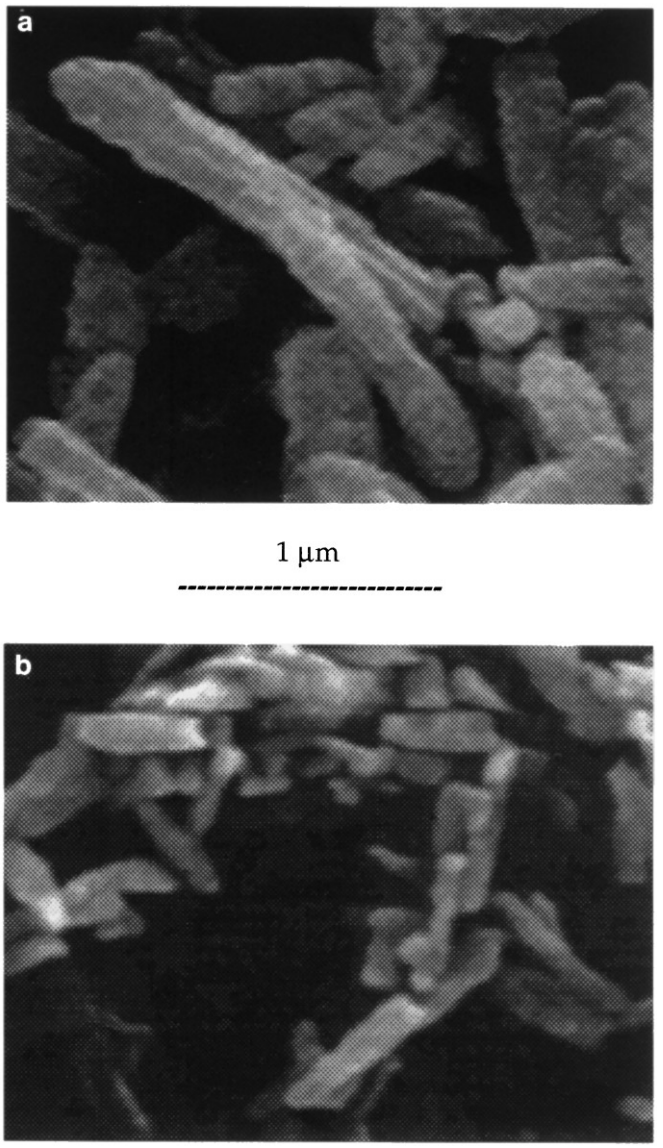

FIG. 1. Scanning electron micrographs of (a) $CuFe_2O_4$ particles and (b) $Cu_{0.67}Co_{0.33}Fe_2O_4$ particles.

25-mm thickness and the isomer shifts are reported with respect to the same. The spectra were computer fitted using a general Lorentzian routine on a VAX 88 system.

EXAFS spectra were recorded with a Rigaku spectrometer with a rotating-anode X-ray generator (Ru-200B, Rigaku, Japan). A Ge(220) crystal was used as the monochromator with a 0.1-mm slit for X-rays from a Mo target. The spectral resolution was about 5 eV at 9-keV incident energy. The ferrites were pressed into self-supporting wafers after mixing with fine polyethylene powder. The thickness of the wafer was adjusted so that the edge jump (μd) in the EXAFS was around 2.0 in every case.

X-ray absorption pre-edge data were collected in steps of 5 eV for 100 eV, and data up to 700 eV after the edge were collected in steps of 1 eV. EXAFS spectra of reference compounds, CuO and Cu_2O, were recorded in a similar way. Fourier transforms of the EXAFS data were obtained with $k_{min} \sim 3.5$ and $k_{max} \sim 11$ Å^{-1} after weighting the data with k^3. McKale's phase and amplitude functions were used for the curve fitting.

DEPENDENCE OF MAGNETIC PROPERTIES ON THE CATION DISTRIBUTION

Copper Ferrite

To investigate the influence of the structure on the magnetic properties, both the SC and Q samples were annealed in air for 20 h at increasing temperatures $T_0, T_1, \ldots, T_i$. After each annealing at $T_0, T_1, \ldots, T_i$, the samples were quenched and their magnetic properties measured at room temperature. Figure 2 shows the variation of coercivity with annealing temperature.

In the case of the SC sample, the coercivity remains constant for annealing temperatures from 25 to 250°C. Above 350°C, the coercive force decreases drastically due to the migration of Cu^{2+} ions from the octahedral to the tetrahedral sites in the spinel lattice, as revealed by the variation of the tetragonal distortion (c/a) of the unit cell (Fig. 3) as well as the saturation magnetization, M_s (Fig. 4).

In the SC sample, the copper ions occupy the octahedral sites of the spinel lattice, leading to a structural formula close to $Fe^{3+}[Cu^{2+}Fe^{3+}]O_4^{2-}$, corresponding to the equilibrium distribution at room temperature. The spinel structure is therefore strongly tetragonally distorted and the c/a ratio has a value of 1.06 ± 0.001. On heating the sample, the copper ions migrate to tetahedral sites and the structural formula of the ferrite changes to $Cu_\alpha^{2+}Fe_{(1-\alpha)}^{3+}[Cu_{(1-\alpha)}^{2+}Fe_{(1+\alpha)}^{3+}]O_4^{2-}$. The resulting decrease in Cu^{2+} ions in the

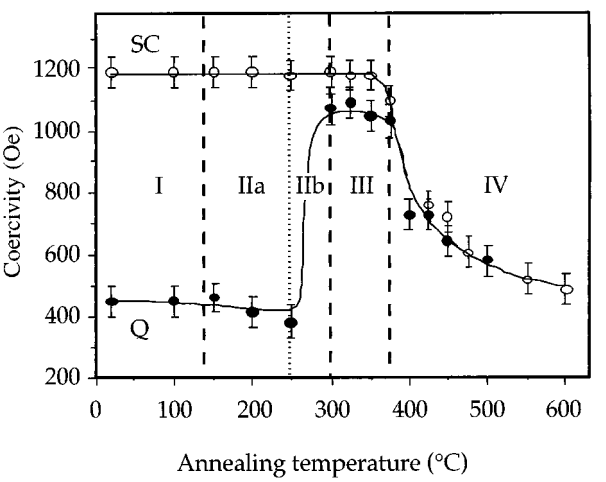

FIG. 2. Variation in coercivity (H_c) with annealing temperature in slow-cooled (SC) and quenched (Q) $CuFe_2O_4$ samples.

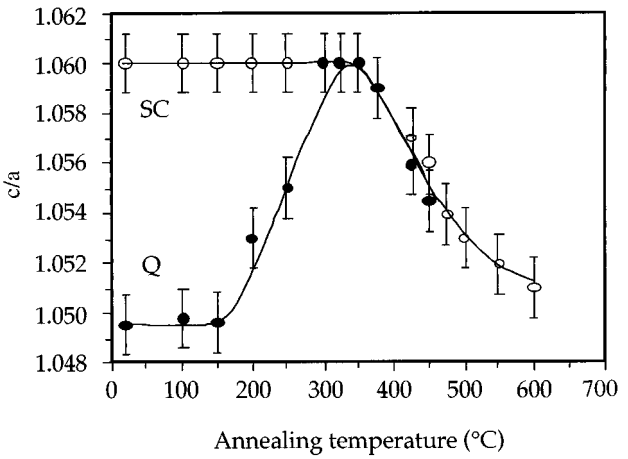

FIG. 3. Variation in tetragonal deformation (c/a) with annealing temperature in slow-cooled (SC) and quenched (Q) $CuFe_2O_4$ samples.

octahedral sites gives rise to a less distorted crystalline structure (5–7). If we assume the magnetic moments of the Fe^{3+} and Cu^{2+} ions to be close to 5 and 1 μ_B, respectively, the saturation magnetization at 0 K for $Cu_{\alpha}^{2+}Fe_{(1-\alpha)}^{3+}[Cu_{(1-\alpha)}^{2+}Fe_{(1+\alpha)}^{3+}]O_4^{2-}$ is expressed by $M_s = \sum$(octahedral sites magnetic moments) $- \sum$(tetrahedral sites magnetic moments) $= (1 + 8\alpha)\,\mu_B$. The migration of Cu^{2+} ions from octahedral to tetrahedral sites increases α and increases the saturation magnetization. The annealing modifies the structural formula of the SC sample only at temperatures higher than 350°C. Above 350°C, we observe a decrease in the c/a ratio (Fig. 3) and an increase in M_s (Fig. 4) due to the migration of Cu^{2+} ions from the octahedral to the tetrahedral sites. The drastic drop in the coercivity (Fig. 2) above 350°C is likely to be the result of the decrease in the crystallographic anisotropy of the unit cell.

Cu*K* XANES measurements were performed on SC and Q samples of $CuFe_2O_4$ as well as on the reference compounds (CuO and Cu_2O). The main peak in both the Q and SC $CuFe_2O_4$ samples was found around the same energy as CuO, implying that the majority of copper ions are in the 2 + state. However, the spectrum of the Q sample showed a slightly more pronounced shoulder on the rising edge of the main peak compared to the SC sample, probably due to the presence of a small proportion of Cu^+ ions.

The Fourier transforms (FT) of the Cu*K* EXAFS of the slow-cooled and the quenched samples are shown in Fig. 5. We see two peaks in each case centered around 1.6 and 2.6 Å. The first peak arises due to Cu–O coordination while the second is due to Cu–Cu(Fe) coordination. Curve-fitting analysis of the inverse transformed data from the first peak (r window: 1.3–2.1 Å) gave a good fit with two sets of Cu–O distances around 2.0 and 2.42 Å, the long distance (2.42 Å) probably originating from the octahedral sites. From Table 2, we see that the coordination number associated with the short distances (2.0 Å) is relatively high in the quenched sample, indicating that the same proportion of copper ions may be frozen in the tetrahedral sites.

From Fig. 2, we see that after the first range of annealing (zone I in Fig. 2), successive annealing at higher temperatures causes a progressive approach toward the equilibrium state (zone II). The IIa region corresponds to the migration of the Cu^{2+} ions from the tetrahedral to the octahedral sites, and the IIb region is related to the oxidation of Cu^+ ions formed in the Q samples due to nonstoichiometry. Calorimetric analysis of the Q samples reveals two exothermic peaks previously ascribed (7) to the migration of the Cu^{2+} ions into the octahedral sublattice

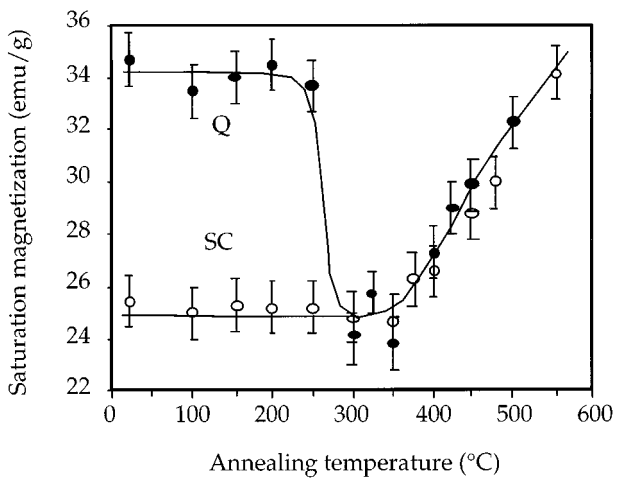

FIG. 4. Variation in saturation magnetization at room temperature in slow-cooled (SC) and quenched (Q) $CuFe_2O_4$ samples.

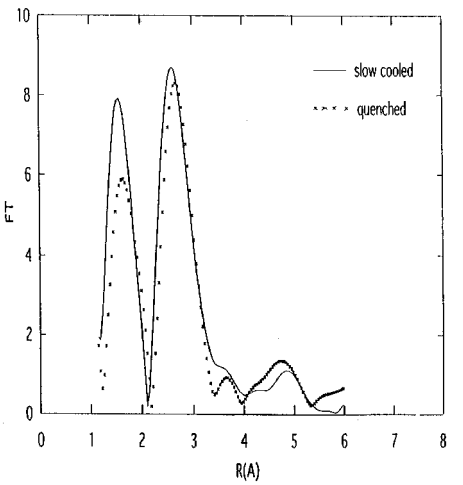

FIG. 5. Fourier transforms of the Cu*K* EXAFS of $CuFe_2O_4$.

TABLE 2
Structure Information Obtained from EXAFS Analysis

Sample	N	R (Å)	$\Delta\sigma$ (Å)	ΔE (eV)
Quenched	5.0	2.0	0.02	6
	1.0	2.42	0.02	6
Slow-cooled	4.0	2.0	0.03	12
	2.0	2.42	0.03	12

and the oxidation of the cuprous ions, respectively. In contrast, the calorimetric curves of the samples after successive annealing show the disappearance of the first peak when annealed in the region IIa, and the disappearance of the second peak when annealed in the region IIb. Furthermore, the formation of octahedral Cu^{2+} ions due to the migration of cupric ions and the oxidation of cuprous ions is confirmed by the increase in the tetragonal distortion (Fig. 3) and also the decrease in the saturation magnetization (Fig. 4). The samples reach an equilibrium state in region III and exhibit the same behavior as the SC samples above 350°C, corresponding to region IV in Fig. 2. Above 350°C, part of Cu^{2+} ions move back to the tetrahedral sites. The variation in the coercivity of the Q samples is roughly related to the distortion of the lattice. The coercivity generally increases with the c/a ratio (Figs. 2 and 3), except in region IIa, where a slight decrease of the coercive force is observed despite the increase of the cell distortion.

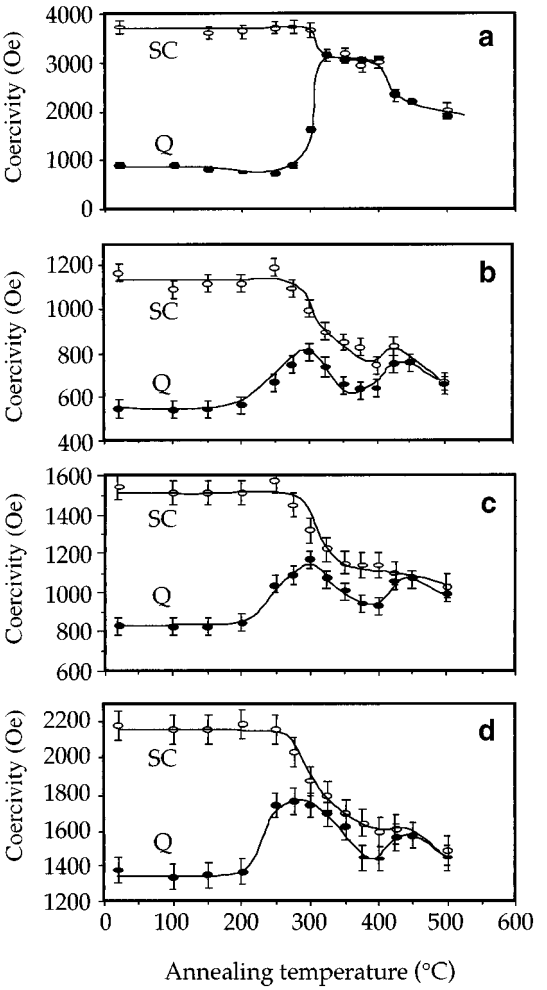

FIG. 6. Variation in coercivity of slow-cooled (SC) and quenched (Q) samples of copper–cobalt ferrite samples: (a) $Cu_{0.85}Co_{0.15}Fe_2O_4$; (b) $Cu_{0.4}Co_{0.6}Fe_2O_4$; (c) $Cu_{0.2}Co_{0.6}Fe_2O_4$; (d) $CoFe_2O_4$.

Mixed Cobalt–Copper Ferrites

The annealing treatments described earlier in the case of copper ferrite were given to the mixed cobalt–copper ferrites as well. For the SC sample of $Cu_{0.85}Co_{0.15}Fe_2O_4$, the first depletion in coercivity is observed close to 300°C and a second one above 400°C (Fig. 6a). From the literature, the first decrease in coercivity is ascribed to the destruction of the directional order established during slow cooling. Furthermore, no significant change in the saturation magnetization is observed in this range of annealing temperatures (Fig. 7), indicating the absence of intersublattice migration. The second decrease may, however, be ascribed to the migration of Cu^{2+} ions from octahedral to tetrahedral sites in the SC $CuFe_2O_4$ sample. The increase in the saturation magnetization found at room temperature is consistent with this interpretation.

The coercivity of Q $Cu_{0.85}Co_{0.15}Fe_2O_4$ exhibits a variation similar to that Q $CuFe_2O_4$ (Fig. 6). However, the big coercivity jump observed at the annealing temperatures of 270 and 310°C can be ascribed to the migration of tetrahedral Cu^{2+} ions into octahedral sites (as revealed by the decrease in saturation magnetization (Fig. 7) as well as to the creation of directional order. There is some evidence for occurrence of directional order in Co-containing spinel ferrites heated at 250–300°C (13–15).

At low annealing temperatures (<400°C), the $H_c = f(T_{\text{annealing}})$ curves in all the mixed Co–Cu ferrites are similar independent of the cobalt content (Fig. 6). At high temperatures, however, a peak in coercivity is seen, especially in the Q samples. This may be ascribed to the migration of the cobalt ions. It is known that Co^{2+} ions are mainly sixfold-coordinated in $CoFe_2O_4$, but some of them are located in tetrahedral sites (21–23). The proportion of the fourfold-coordinated Co^{2+} ions is an important as the quenching temperature (24). The peak in coercivity at an annealing temperature of 450°C may be interpreted as follows (Fig. 6).

Annealing between 400 and 450°C gives sufficient energy to displace the Co^{2+} ions from the tetrahedral sites to the octahedral sites. The resulting coercivity enhancement is all

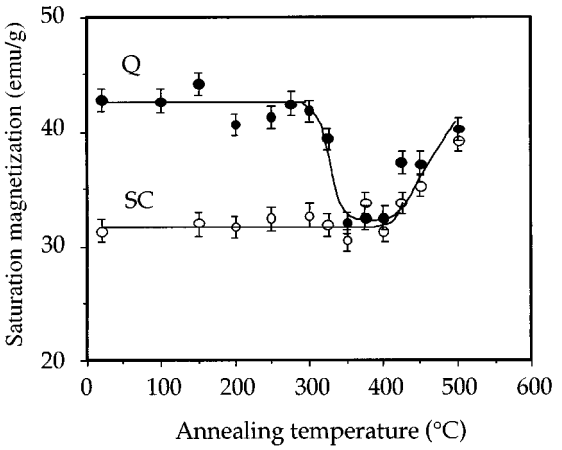

FIG. 7. Variation in saturation magnetization at room temperature in slow-cooled (SC) and quenched (Q) samples of $Cu_{0.85}Co_{0.15}Fe_2O_4$.

the more prominent since a large proportion of the Co^{2+} ions are displaced. This is why the greatest coercivity variations are observed for the Q samples wherein the cation distribution is far from equilibrium. Above 450°C, the thermal energy allows the destruction of the equilibrium state and the Co^{2+} ions also migrate from the octahedral to the tetrahedral sites. Accordingly, SC and Q samples show the same behavior in this range of temperature. Mössbauer spectra of $CoFe_2O_4$ (Fig. 8 and Table 3) do not show any significant difference in the samples annealed at 400–450°C. In this respect, measurement of the coercivity is more sensitive than the Mössbauer spectra to reveal cation migration.

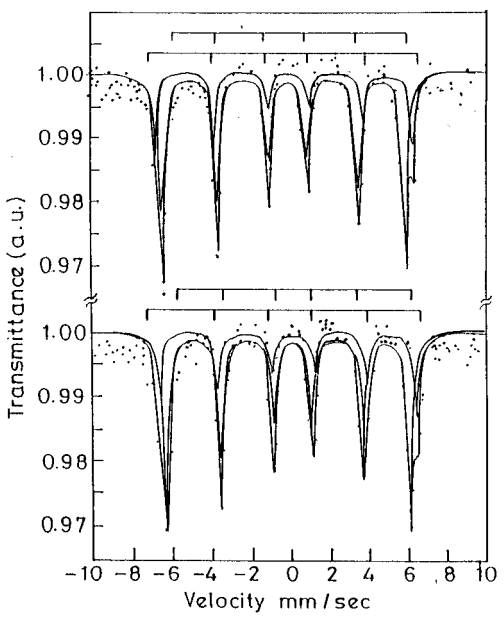

FIG. 8. Mössbauer spectra of quenched (Q) $CoFe_2O_4$ samples after annealing at 400 and 450°C.

TABLE 3
Mössbauer Spectroscopic Measurements on $CoFe_2O_4$

Annealing temperature (°C)	Isomer shift (mm/s)		Internal magnetic field (kOe)		Area	
	A	*B*	*A*	*B*	*A*	*B*
400	0.29	0.24	512	485	1.0	2.8
450	0.24	0.24	512	485	1.0	2.9

Because of the directional ordering discussed earlier, the coercivity of the quenched $CoFe_2O_4$ sample reaches a maximum value for a temperature close to 275°C. In the other samples, the increase in coercivity occurs above this temperature because of the cupric ion migration. Such an increase in coercivity occurs not only when the migration gives rise to or favors the tetragonal distortion of the lattice but also when the unit cell remains cubic. It therefore seems that the local deformation of the lattice due to the distorted octahedral sites containing Cu^{2+} ions suffices to produce magnetoelastic effects responsible for the enhancement of the coercivity.

OPTICAL PROPERTIES AND CATIONIC DISTRIBUTION

Near-IR–Visible absorption spectroscopic measurements allow us to verify the conclusions deduced from the study of magnetic properties of $CoFe_2O_4$, $CuFe_2O_4$, and $Co_xCu_{1-x}Fe_2O_4$. The optical properties of cobalt(II), copper(II), and iron(III) in reference compounds are presented in Table 4. In Figs. 9 and 10, we present the electronic spectra of $CuFe_2O_4$ and $CoFe_2O_4$. The copper(II) in $CuFe_2O_4$ may be characterized by the band at 6000 cm^{-1} (1650 nm) corresponding to the t_3 and o_1 transitions. As expected in such paramagnetic spinels, the absorption coefficient k for the Cu^{2+} ion in tetrahedral coordination is 10 times higher than that of octahedral Cu^{2+}. Bands at energies higher than 16,000 cm^{-1} are more intense than the transitions related to the $(t_{2g}^{\alpha})^3(e_g^{\alpha})^1(t_{2g}^{\beta})^1$ configuration and give a steep absorption edge. In inverse ferrites (25), a band near 19,000 cm^{-1} is unambiguously assigned to a composite of the $^6A_1 \rightarrow {}^4T_2({}^4G)$ ligand field transition of tetrahedral Fe^{3+} and $^6A_1 + {}^6A_1 \rightarrow {}^4T_2 + {}^4T_2({}^4G)$ pair transitions. In these compounds, the *A–B* antiferromagnetic interaction enhances the intensity of the ligand field transition.

Tetrahedral cobalt(II) is identifiable by means of the $^4A_2 \rightarrow {}^4T_1({}^4F)$ transition in the range 6000–7500 cm^{-1} (1650–1350 nm). In the electronic spectrum of $CoFe_2O_4$, the absorption edge is shifted to lower energies. The strong absorption at about 14,000 cm^{-1} (700 nm) is due to the overlapping of the $^4A_2 \rightarrow {}^4T_1({}^4P)$ transition of the tetrahedral Co^{2+} ions and the $Co^{2+} + Fe^{3+} \rightarrow Co^{3+} + Fe^{2+}$ metal–metal charge transfer transition (26–28). The vari-

TABLE 4
Energies and Assignments of Bands Observed in Reference Spinels

Species	Energies observed electronic transitions ($10^3\,cm^{-1}$) and				Optical parameters	
					$\Delta = 10Dq$	B
$Co^{2+}T_d$ ($\sim 25\%$) in $CoGa_2O_4$	6.7[a] $^4A_2 \rightarrow {}^4T_1({}^4F)$	16.6[a] $^2A_2 \rightarrow {}^4T_1({}^4P)$			3.85	0.785
Cu^{2+} in $CuGa_2O_4$	T_d (20%), 3.6 $({}^2B_2 \rightarrow {}^2E_1)_1t_1$ O_h (80%) $B_{1g} \rightarrow A_{1g}o_1$	6.15 $({}^2B_2 \rightarrow {}^2A_1)_1t_3$ 6.15 (11) $B_{1g} \rightarrow B_{2g}o_2$	12.5 $E_g o_3$	*22* LMCT 32 LMCT	3.8	
Fe^{2+} in $MgFe_2O_4$	10.3 $^6A_1 \rightarrow {}^4T_1 o_h$	(16.2) $^6A_1 \rightarrow {}^4T_1T_d$	18.8 $^6A_1 \rightarrow {}^4T_2T_d$ $2({}^6A_1) \rightarrow 2({}^4T_1)$	21.5 $^6A_1 \rightarrow {}^4E_1, {}^4A_1$		

[a]Energy of the barycenter of the three quartet states.

ation in the absorption at 1650 nm with annealing treatment was investigated for quenched $CoFe_2O_4$ as well as for quenched and slowly cooled $CuFe_2O_4$ samples (Table 5). A comparison of the experimental data on copper ferrite with the data for mixed copper ferrites prepared by the usual ceramic method (29, 30) leads to the conclusion that in the SC sample and the Q sample annealed at 500°C, $\sim 10\%$ of the Cu^{2+} ions are in tetrahedral coordination. Heat treatment of the quenched samples at 300°C induces the migration of the Cu^{2+} ions from the tetrahedral to the octahedral sites. The decrease in the optical absorption and the increase in the coercivity found in $CoFe_2O_4$ samples annealed around 425–450°C are explained on the basis of the migration of Co^{2+} ions from the tetrahedral to the octahedral sites. Above 450°C, an inverse migration is observed.

Two peaks in coercivity were observed at 275–300°C and 450°C in the case of $CoFe_2O_4$ (Fig. 6d) as well as the Q samples of mixed Co–Cu ferrites (Figs. 6b and 6c). The correlation between coercivity and optical measurements is presented Table 6. The first peak is ascribed to the development of directional order and the second to the migration of Co^{2+} from the tetrahedral to the octahedral sites. Creation of directional order is known to induce an enhancement of the tetrahedral cobalt(II) ligand field transition in $CoFe_2O_4$ (31).

CONCLUSIONS

Cu(II) and Co(II) ions do not have a strong site preference in the spinel structure. Consequently, $Co_xCu_{1-x}Fe_2O_4$ with different cation distributions are observed, depending on the thermal history. The cation distributions in $Co_xCu_{1-x}Fe_2O_4$ particles, slowly cooled or quenched from 710°C, are modified by cation migration caused by successive annealing. In the slowly cooled samples, three types of migration

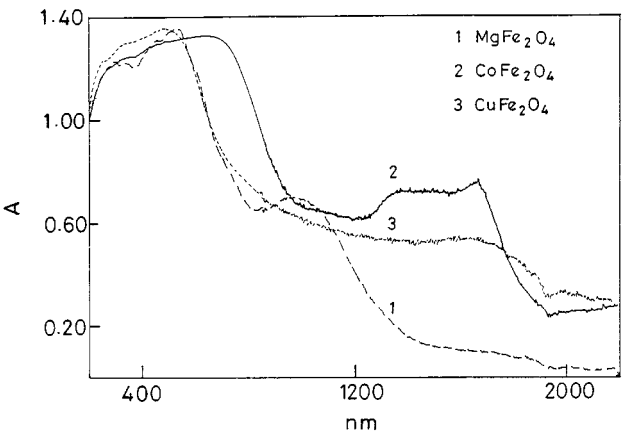

FIG. 9. UV–vis–near-IR absorption spectra of MFe_2O_4 ferrites: M = Mg (1), Co (2), and Cu (3).

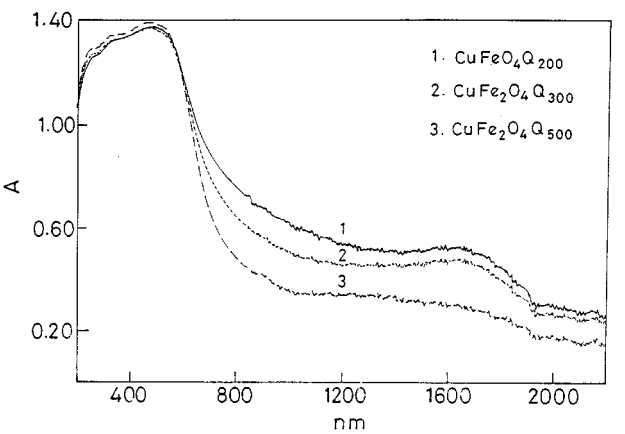

FIG. 10. Influence of annealing temperature on the near-IR band of Q $CuFe_2O_4$ samples.

TABLE 5
Analysis of the Cationic Migration by Optical Measurements for Copper and Cobalt Ferrites

		Annealing temperature (°C)					
Compound	Parameter[a]	100	200	300	400	450	500
$CoFe_2O_4$, Q	$F(R)$		3.5	3.7	3.71	3.10	3.49
	H_c (Oe)		1360	1740	1395	1490	1405
$CuFe_2O_4$, SC	A	0.09		0.10	0.16		0.20
	H_c (Oe)	1190		1190	870		580
$CuFe_2O_4$, Q	A		0.20	0.10	0.13		0.20
	H_c (Oe)		415	1070	730		580

[a] H_c, coercivity; $F(R)$; Kubelka–Munk function; A; absorbance.

are observed. The first one, occurring above 350°C, is due to the displacement of the octahedral cupric ions to the tetrahedral sites. From 400 to 450°C, some of the Co^{2+} ions which were not stabilized in the octahedral sites during the slow cooling migrate into the octahedral sites. The cobalt ions, however, are displaced from their stable coordination by annealing carried out above 450°C. In the quenched samples, Cu^{2+} ions move from the tetrahedral to the octahedral sites from 150 to 250°C and the Cu^{+} ions are oxidized between 250 and 300°C. The quenched samples annealed from 300 to 350°C have a cation distribution close to that of the slowly cooled particles. Above 350°C, the slowly cooled and the quenched samples exhibit a similar behavior.

The magnetic anisotropy of acicular $Co_xCu_{1-x}Fe_2O_4$ particles depends on the location of both the cupric and cobaltous ions. The strengthening of the magnetic anisotropy results from the distortion of the spinel lattice due to the cooperative Jahn–Teller effect of the octahedral cupric ions, on the one hand, and the coordination and directional ordering of the cobaltous ions, on the other. Because of the strong dependence of the anisotropy on the location of cations, the measurement of coercivity is a sensitive probe for following cation migrations after successive annealing. Furthermore, the distortion of the unit cell, the directional order of the octahedral Co^{2+} ions, and the shape anisotropy of the particles combine to render $Co_xCu_{1-x}Fe_2O_4$ ferrite powders to become very hard magnetic materials with coercivities up to 4000 Oe.

TABLE 6
Correlation between Coercivity and Optical Absorption

		Absorption (in $F(R)$ at 1650 nm) for $Co_{0.6}Cu_{0.4}Fe_2O_4$ annealed at different temperatures				
	Parameter	100°C	300°C	400°C	450°C	500°C
SC sample	$F(R)$	1.92	1.83	1.79	1.76	2.14
	H_c (Oe)	1095	1000	750	835	660
Q sample	$F(R)$	2.1	2.54	2.09	1.78	2.05
	H_c (Oe)	545	810	635	755	660

ACKNOWLEDGMENT

The authors thank the Indo-French Centre for Promotion of Advanced Scientific Research, New Delhi, for support of this research.

REFERENCES

1. L. Weil, F. Bertaut, and L. Bochirol, *J. Phys. Radium* **11,** 208 (1950).
2. H. M. O'Bryan, H. J. Levinstein, and R. C. Sherwood, *J. Appl. Phys.* **37,** 437 (1966).
3. J. Janicki, J. Pietrzak, A. Porebska, and J. Suwalski, *Phys. Status Solidi A* **72,** 95 (1982).
4. H. A. Jahn and E. Teller, *Proc. R. Soc. London* **161,** 220 (1937).
5. P. J. Wojtowicz, *Phys. Rev.* **116,** 32 (1959).
6. J. Mexmain, *Ann. Chim.* **4,** 429 (1969).
7. C. Villette, Ph. Tailhades, and A. Rousset, *J. Solid State Chem.* **117,** 64 (1995).
8. A. d'Huysser, R. Lerebours-Hannoyer, M. Lenglet, and J. P. Bonnelle, *J. Solid State Chem.* **39,** 246 (1981).
9. X. X. T. Tang, A. Manthiram, and J. B. Goodenough, *J. Solid State Chem.* **79,** 250 (1989).
10. L. Néel, *J. Phys. Radium* **15,** 225 (1954).
11. S. Chikazumi, "Physics of Magnetism," Chap. 17, John Wiley, New York, 1964.
12. J. C. Slonczewski, *Phys. Rev.* **110,** 1341 (1958).
13. Ph. Tailhades, P. Mollard, A. Rousset, and M. Gougeon, *IEEE Trans. Magn.* **26,** 1822 (1990).
14. M. C. Deng and T. S. Chin, *Jpn. J. Appl. Phys.* **30,** 1276 (1991).
15. Ph. Tailhades, L. Bouet, B. Gillot, P. Mollard, and A. Rousset, *Proc. Int. Conf. Ferrites, 6th* 991 (1992).
16. P. Mollard, Ph. Tailhades, and A. Rousset, *IEEE Trans. Magn.*, **26,** 241 (1990).
17. Ph. Tailhades, Thesis, Toulouse, France, 1988.
18. R. Deyrieux and A. Peneloux, *Bull. Soc. Chim. Fr.* 2675 (1969).
19. A. M. Berkowitz and W. J. Scheule, *J. Appl. Phys.* **30,** 1345 (1959).
20. H. Fichtner-Schmittler, *Cryst. Res. Technol.* **19,** 1225 (1984).
21. G. A. Sawatsky, F. van der Woude, and A. H. Morrish, *J. Appl. Phys.* **39,** 1204 (1968).
22. P. J. Murray and J. W. Linnett, *J. Phys. Chem. Solids* **37,** 1041 (1976).
23. H. L. Yakel, *J. Phys. Chem. Solids* **41,** 1097 (1980).
24. M. R. De Guire, R. C. O'Handley, and G. Kalonji, *J. Appl. Phys.* **65,** 3167 (1989).
25. F. Hochu, M. Lenglet, and C. K. Jørgensen, *J. Solid State Chem.* **120,** 244 (1995).
26. M. Lenglet, F. Hochu, and J. Dürr, *J. Physique IV* **7,** C1/259 (1997).
27. M. Abe and M. Gomi, *J. Appl. Phys.* **53,** 8172 (1982).
28. W. L. Peters and J. W. D. Martens, *J. Appl. Phys.* **53,** 8172 (1982).
29. J. Lopitaux, A. Erb, M. Lensen, J. Hubsch, and M. Lenglet, *Rev. Chim. Miner.* **13**, 397 (1976).
30. M. Lenglet, P. Foulatier, J. Dürr, and J. Arsene, *Phys. Status Solidi A* **94,** 461 (1986).
31. M. Lenglet, B. Lefez, B. Hannoyer, L. Presmanes, Ph. Tailhades, and A. Rousset, Presented at the ECSSC 95, September 1995, Montpellier, France.